# A dimeric equilibrium intermediate nucleates Drp1 reassembly on mitochondrial membranes for fission

Patrick J. Macdonald[a,*], Natalia Stepanyants[a,*], Niharika Mehrotra[a], Jason A. Mears[b,c], Xin Qi[a,c], Hiromi Sesaki[d], and Rajesh Ramachandran[a]

[a]Department of Physiology and Biophysics, [b]Department of Pharmacology, and [c]Center for Mitochondrial Diseases, Case Western Reserve University School of Medicine, Cleveland, OH 44106; [d]Department of Cell Biology, Johns Hopkins University School of Medicine, Baltimore, MD 21205

**ABSTRACT** **The GTPase dynamin-related protein 1 (Drp1) catalyzes mitochondrial division, but the mechanisms remain poorly understood. Much of what is attributed to Drp1's mechanism of action in mitochondrial membrane fission parallels that of prototypical dynamin in endocytic vesicle scission. Unlike the case for dynamin, however, no lipid target for Drp1 activation at the mitochondria has been identified. In addition, the oligomerization properties of Drp1 have not been well established. We show that the mitochondria-specific lipid cardiolipin is a potent stimulator of Drp1 GTPase activity, as well as of membrane tubulation. We establish further that under physiological conditions, Drp1 coexists as two morphologically distinct polymeric species, one nucleotide bound in solution and the other membrane associated, which equilibrate via a dimeric assembly intermediate. With two mutations, C300A and C505A, that shift Drp1 polymerization equilibria in opposite directions, we demonstrate that dimers, and not multimers, potentiate the reassembly and reorganization of Drp1 for mitochondrial membrane remodeling both in vitro and in vivo.**

**Monitoring Editor**
Thomas D. Fox
Cornell University

Received: Feb 7, 2014
Revised: Apr 14, 2014
Accepted: Apr 21, 2014

## INTRODUCTION

The mitochondria of eukaryotic cells form elaborate networks of branched, tubular structures that constantly undergo fission and fusion (Chan, 2012). A delicate balance of these counteracting processes is essential for the maintenance of mitochondrial size, distribution, homogeneity, and inheritance (Okamoto and Shaw, 2005; Youle and van der Bliek, 2012; Friedman and Nunnari, 2014). In addition, mitochondrial dynamics are intricately linked to apoptosis (Hoppins and Nunnari, 2012). Emerging evidence indicates that defects in mitochondrial dynamics precipitate neurodegenerative diseases such as Alzheimer's, Huntington's, and Parkinson's (Itoh *et al.*, 2013) and may be critically involved in cardiac dysfunction (Ong and Hausenloy, 2010).

Dynamin-related protein 1 (Drp1; Figure 1A) mediates mitochondrial membrane fission (Bui and Shaw, 2013; Elgass *et al.*, 2013). Located predominantly in the cytosol, Drp1, in response to a variety of physiological cues, is recruited to the outer mitochondrial membrane (OMM), where it presumably organizes into a large helical polymer that wraps around the organelle at discrete, predetermined division sites (Friedman *et al.*, 2011; Korobova *et al.*, 2013). Here Drp1 is believed to exert its mechanochemical activity by constricting the mitochondrial double membrane to the point of fission. Drp1 targeting to potential mitochondrial division sites is facilitated through interactions with OMM-anchored adaptor proteins such as fission factor 1 (Fis1), mitochondrial fission factor (Mff), and mitochondrial dynamics proteins of 49 and 51 kDa (MiD49/51; Loson *et al.*, 2013).

Our mechanistic understanding of how Drp1 mediates membrane fission stems primarily from in vitro studies of its yeast homologue, Dnm1p (Lackner and Nunnari, 2009). Purified Dnm1p, which

This article was published online ahead of print in MBoC in Press (http://www.molbiolcell.org/cgi/doi/10.1091/mbc.E14-02-0728) on April 30, 2014.

*These authors contributed equally to this work.

Address correspondence to: Rajesh Ramachandran (rxr275@case.edu).

Abbreviations used: CL, cardiolipin; Drp1, dynamin-related protein 1; Fis1, fission factor 1; FRET, Förster resonance energy transfer; GUV, giant unilamellar vesicle; MALS, multiangle light scattering; MiD 49/51, mitochondrial dynamics proteins of 49/51 kDa; Mff, mitochondrial fission factor; OMM, outer mitochondrial membrane; PA, phosphatidic acid; PC, phosphatidylcholine; PE, phosphatidylethanolamine; PS, phosphatidylserine; SEC, size-exclusion chromatography; WT, wild type.

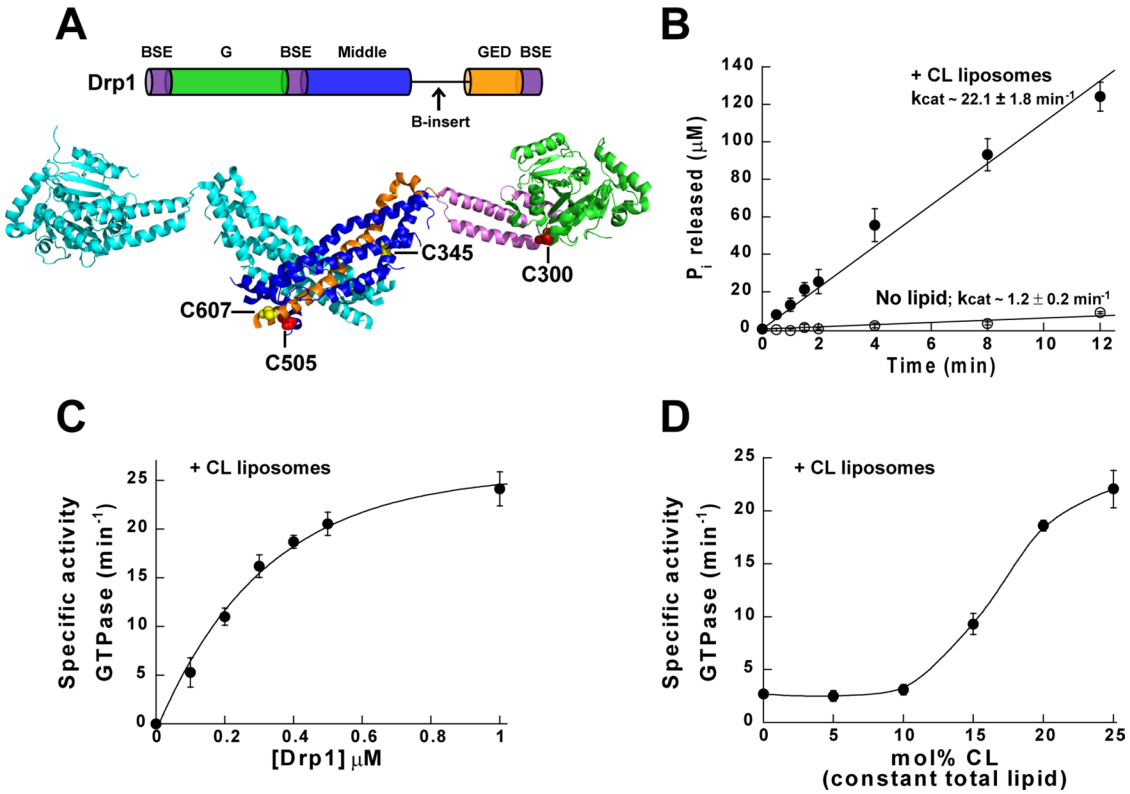


FIGURE 1: Cardiolipin potently stimulates Drp1 GTPase activity. (A) Domain architecture of Drp1 and a color-coded representation of a monomer in the dimer crystal structure (Protein Data Bank ID 4BEJ). Residues mutated in this study are indicated and represented in space-fill. BSE, bundle signaling element; G, GTPase domain; GED; GTPase effector domain. (B) GTPase activity of Drp1 (0.5 μM) in the absence and presence of CL-containing liposomes (150 μM total lipid) plotted as concentration of $P_i$ released over time. The average turnover number ($k_{cat}$) ± SD is indicated. (C) Specific activity of Drp1 on CL-containing liposomes (150 μM total lipid) as a function of protein concentration. Average ± SD for $n \geq 3$. (D) Specific activity of Drp1 (0.5 μM) on CL-containing liposomes (150 μM total lipid) as a function of mole percent CL content. Average ± SD for $n \geq 3$.

exists as multimers in solution, propagates into helical polymers of diameter comparable to mitochondrial division sites in vivo when assembled onto membrane tubules derived from negatively charged liposomes (Ingerman *et al.*, 2005). Cooperative GTP hydrolysis triggers a large, concerted conformational rearrangement in the preassembled Drp1 polymer, which mechanochemically constricts the underlying membrane tubule and poises it for fission, similar in principle to prototypical dynamin in endocytic vesicle scission (Mears *et al.*, 2011). Mutations that limit Dnm1p self-assembly to a terminal dimer in solution also impair helical propagation and cooperative GTPase stimulation (Ingerman *et al.*, 2005).

By contrast, the oligomerization properties of mammalian Drp1 appear distinct. However, these have not been unambiguously established. Mammalian Drp1 reportedly exists in solution as stable dimers (Koirala *et al.*, 2013), tetramers (Yoon *et al.*, 2001; Bossy *et al.*, 2010), or in dynamic dimer–tetramer equilibrium (Chang *et al.*, 2010; Frohlich *et al.*, 2013). Furthermore, Drp1 helices formed in the presence of GTP analogues in solution (~30–50 nm diameter), unlike those of Dnm1p (Ingerman *et al.*, 2005), appear morphologically distinct from the corresponding helices formed on negatively charged membrane templates, which can vary greatly in diameter from 30 to >150 nm, depending on the Drp1 isoform and/or conditions used (Yoon *et al.*, 2001; Bossy *et al.*, 2010; Frohlich *et al.*, 2013; Koirala *et al.*, 2013). Whether these differences reflect isoform-specific properties of Drp1 (Strack *et al.*, 2013) and/or the inherent property of the pure phosphatidylserine (PS) liposomes used to undergo variable shape transformations (Hauser and Phillips, 1973; Fuller *et al.*, 2003) is yet to be determined. Moreover, although the functional significance of distinct Drp1 polymerization in solution versus that on membranes remains to be established, it is unclear whether Drp1 multimerization in solution is essential for nucleation of Drp1 higher-order self-assembly on membranes (Ingerman *et al.*, 2005; Bhar *et al.*, 2006).

Here we report that the mitochondria-localized lipid cardiolipin potently activates Drp1 and supports membrane tubulation. With the identification and characterization of two new mutants, we further reveal that Drp1 exists in dynamic equilibrium between two morphologically distinct oligomeric states in the cell, one in the cytosol and the other localized on mitochondrial membranes, which equilibrate via a dimeric assembly intermediate. We show that dimers, and not multimers, potentiate the assembly and reorganization of Drp1 on mitochondria for membrane remodeling and fission.

## RESULTS

### Cardiolipin is a potent stimulator of Drp1 GTPase activity

Although pure PS liposomes are routinely used as templates for assaying Drp1 activity in vitro, this lipid is essentially absent (~1 mol%) at the mitochondria (Kagan *et al.*, 2005; van Meer *et al.*, 2008; Horvath and Daum, 2013). OMM-mimetic liposomes composed of a variety of negatively charged lipids were shown to bind and enzymatically stimulate yeast Dnm1p, but the activating lipid target(s) were obscure (Lackner *et al.*, 2009). Through an extensive lipid

screen (Supplemental Figure S1A), we identified the negatively charged, mitochondria-specific lipid cardiolipin to be the most potent stimulator of Drp1's cooperative GTPase activity on membranes (Figure 1, B and C). Cardiolipin (CL), found predominantly in the inner mitochondrial membrane (IMM), is reportedly enriched at "contact sites" between the IMM and OMM at concentrations up to 25 mol% (Ardail *et al.*, 1990; Schlattner *et al.*, 2014; Tatsuta *et al.*, 2014). This corresponded to the typical CL content of our "contact site" biomimetic liposomes. No stimulation observed for Drp1 at CL concentrations ≤10 mol% suggested that "CL-enriched microdomains" at the OMM may indeed function as "recruitment platforms" for Drp1 activation (Sorice *et al.*, 2009; Figure 1D). At an equivalent mole fraction, PS did not substantially increase Drp1 GTPase activity (Supplemental Figure S1A). Other negatively charged lipid species present at the OMM, namely phosphatidic acid (PA) and phosphatidylglycerol (PG), enhanced Drp1 GTPase activity, although not nearly to the same extent as CL (Supplemental Figure S1A).

We next investigated Drp1 in the presence of various phosphoinositides to determine whether the extent of Drp1 GTPase stimulation was positively correlated with the negative charge density of lipid headgroups. A recently proposed role for Drp1 in synaptic vesicle endocytosis also suggests a likely interaction with phosphoinositides at the plasma membrane (Li *et al.*, 2013). Remarkably, no such correlation was evident (Supplemental Figure S1B). Indeed, phosphatidylinositol-4-phosphate (PI4P) was substantially more effective than the more negatively charged phosphatidylinositol-4,5-bisphosphate ($PI4,5P_2$) in stimulating Drp1 GTPase activity. Phosphatidylinositol (PI) of negative charge density lower than PI4P was, on the other hand, ineffective. Although the physiological relevance of these findings remains to be established, our data nevertheless indicate that CL is a mitochondria-specific, lipid stimulator of Drp1 GTPase activity and that Drp1 recognition of CL is not solely based on headgroup negative charge density.

### Drp1 tubulates CL-containing liposomes

A previous study postulated that Drp1 mediates mitochondrial membrane fission by catalyzing the formation of a hemi-fusion/fission intermediate in a CL-dependent manner (Montessuit *et al.*, 2010). However, no membrane constriction or tubulation necessary for such an event was apparent in that study. Instead, Drp1 activity was limited to the tethering and hemifusion of freely suspended liposomes. Moreover, under the conditions used, neither higher-order Drp1 self-assembly nor assembly-dependent stimulation of GTPase activity on CL-containing liposomes was evident. We therefore reevaluated the behavior of Drp1 on CL-containing liposomes.

To this end, we used a system of surface-immobilized giant unilamellar vesicles (GUVs) as model membrane templates to visualize Drp1-mediated membrane remodeling in real time. We indeed found that Drp1 was recruited to the GUV membrane surface in a CL-dependent manner (Figure 2A). Extensive remodeling of the membrane into narrow, protein-coated membrane tubules, however, further ensued (Figure 2B and Supplemental Figure S2). This phenomenon was not observed previously (Montessuit *et al.*, 2010).

Electron microscopy (EM) examination of the membrane tubule ultrastructure revealed a uniform pattern of helical Drp1 self-assembly that approximated 100–150 nm in diameter (Figure 2C). These dimensions were comparable to the diameter of mitochondrial constriction sites observed in vivo (Ingerman *et al.*, 2005; Friedman *et al.*, 2011).

On pure PS liposomes, Drp1 formed helices of mostly comparable diameter (Supplemental Figure S3A). However, helical regions of highly variable diameter were also evident (Supplemental Figure S3A), indicating that use of this inherently transformable membrane template may partially account for the observed differences in membrane tubule diameters for the same, or between different, Drp1 isoform(s) in independent studies (compare our results with those of Frohlich *et al.*, 2013, and Koirala *et al.*, 2013). That Drp1 could form curvature-adaptable polymers on membranes was further evident from its helical assembly on preformed CL-containing lipid nanotubes of ~30 nm diameter (Supplemental Figure S3B).

### Drp1 constitutes two morphologically distinct polymers

Drp1 reportedly forms helical polymers of uniformly narrow diameter (~30 nm) on PS membrane tubules when either GTPγS, a slowly hydrolyzable GTP analogue (Yoon *et al.*, 2001), or GTP (Koirala *et al.*, 2013) is added. Drp1 can indeed form polymers of similar diameters in solution even in the absence of a membrane template when either GMP-PCP, a nonhydrolyzable GTP analogue (Figure 3A), or GTPγS (Yoon *et al.*, 2001; Bossy *et al.*, 2010; Koirala *et al.*, 2013) is present. To determine whether GTP binding causes a pronounced constriction of the proportionally large, membrane-bound Drp1 helical polymer to approach the very narrow diameters found for Drp1 helices in solution, we incubated Drp1 with CL-containing liposomes in the presence of GMP-PCP. Remarkably, GMP-PCP did not elicit any such constriction (Figure 3B). This result was indeed similar to that previously observed for yeast Dnm1p (Mears *et al.*, 2011). Instead, we observed the emergence of a substantial fraction of the tightly wound, helical polymers described earlier for Drp1 in solution (Figure 3B). The coexistence of these morphologically distinct species under steady-state conditions suggested that Drp1 populates two polymeric states, one in solution and the other membrane associated, which relate via dynamic equilibrium. To ascertain this possibility, we next investigated the polymerization equilibria of Drp1.

### Drp1 displays complex polymerization equilibria in solution

Size-exclusion chromatography (SEC) under physiological ionic strength conditions (150 mM KCl in buffer solution) revealed a very broad elution spectrum for Drp1 wild type (WT; Figure 4A, top). These data indicated that Drp1 exists in a fast dynamic equilibrium between multiple oligomeric states in solution. The existence of such equilibria was evident from consequent shifts in the Drp1 WT SEC elution profile as a function of loaded protein concentration (Figure 4B, top).

In a screen for mutants that slightly altered Drp1 polymerization equilibria but were otherwise comparable to WT in enzymatic activity (Supplemental Figure S4), we identified Drp1 C345A and C607A. Native Cys residues were substituted, as their electrophilic modifications were shown to alter Drp1 oligomerization (Cho *et al.*, 2009; Mishra *et al.*, 2010). Fortuitously, these mutants exhibited discernible peaks within their broad SEC elution profiles (Figure 4A, middle). Coupled multiangle light scattering (MALS) measurements (see *Materials and Methods* for a description) of the various peaks within revealed that Drp1 exists in a dynamic, dimer–oligomer equilibrium in solution and propagates in quantized dimeric increments (Figure 4A, middle, right axis). Thus the minimal functional assembly subunit of Drp1 under physiological conditions is a dimer, and not a tetramer, as previously suggested.

We also identified two additional mutants of Drp1, C300A and C505A (Figure 1A), that exhibited dramatically altered oligomerization properties relative to WT (Figure 4A, bottom). SEC-MALS analyses revealed that Drp1 C300A was supra-oligomeric in solution, with a greater propensity to form higher-order structures even at low

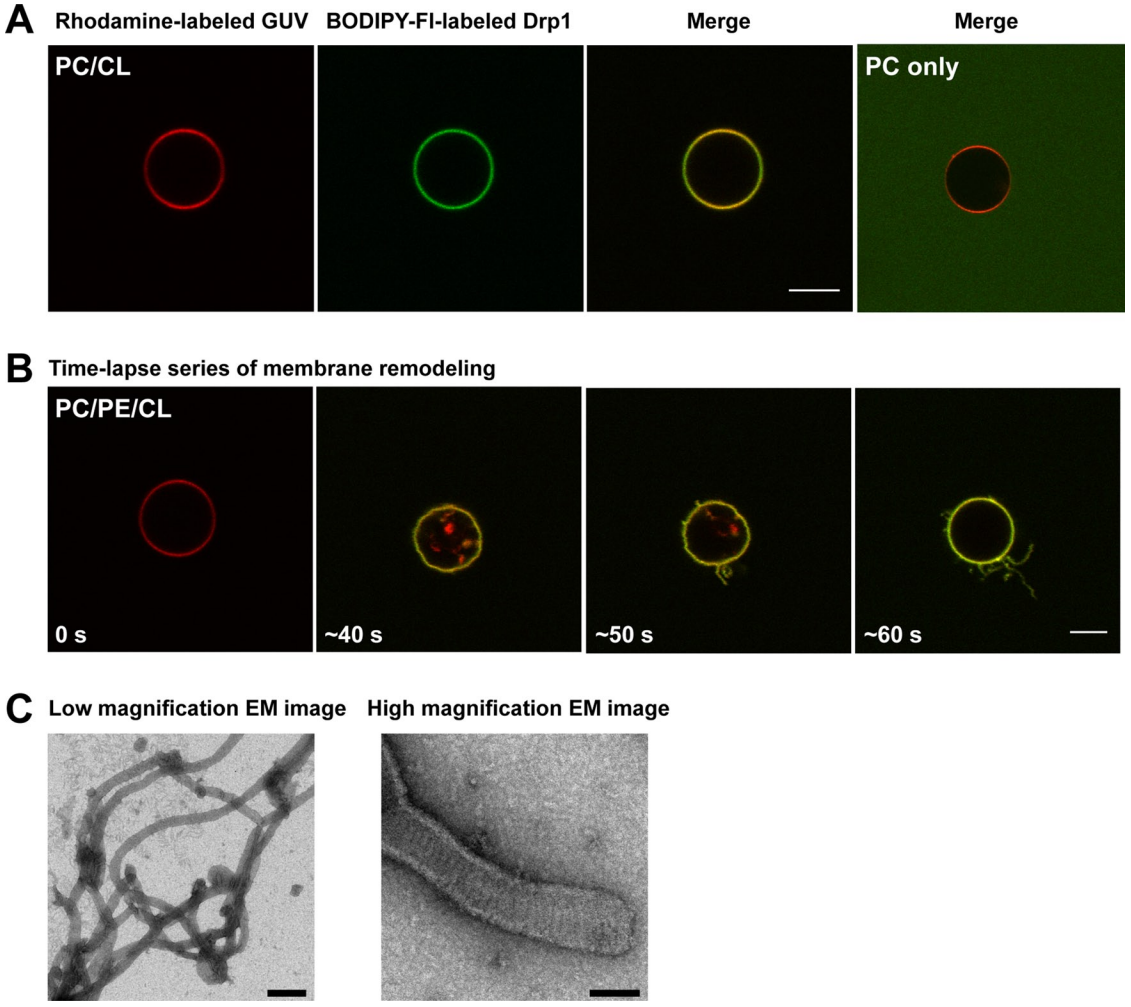


FIGURE 2: Drp1 efficiently remodels CL-containing membranes. (A) Binding of BODIPY-labeled Drp1 (green channel) to PC/CL-containing, rhodamine-labeled GUVs (red channel). PC-only control GUVs do not bind Drp1. The final Drp1 concentration was 0.5 μM. Scale bar, 5 μm. (B) Time-lapse series of membrane tubulation by BODIPY-Fl–labeled Drp1 (0.5 μM protein final) on rhodamine-labeled PC/PE/CL GUVs. Scale bar, 5 μm. (C) Representative low- magnification (scale bar, 500 nm) and high-magnification (scale bar, 100 nm) EM images of Drp1-decorated membrane tubules.

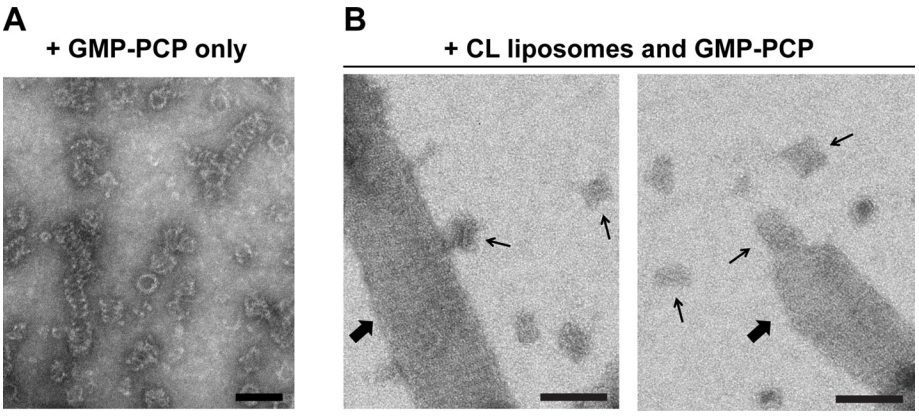


FIGURE 3: Morphologically distinct polymers of Drp1. (A) Tightly wound helical polymers of Drp1 formed in the presence of GMP-PCP in solution. (B) Coexisting solution-suspended (slender arrows) and membrane-associated (block arrows) helical polymers of Drp1 found in the presence of GMP-PCP and CL-containing liposomes. Representative EM images. Scale bar, 100 nm.

protein concentrations (Figure 4B, middle). Drp1 C505A, on the other hand, was predominantly dimeric in solution even at relatively high protein concentrations (Figure 4B, bottom). Nevertheless, both mutants exhibited robust polymerization equilibrium dynamics with respect to protein concentration.

In the presence of GMP-PCP, both Drp1 C300A and Drp1 C505A constituted helical polymers in solution (Figure 4C), albeit with varied efficiencies relative to WT. In centrifugation assays that reliably sediment these high-density protein polymers, both mutants appeared partially impaired relative to WT (Figure 4D), indicating that altered local structural dynamics caused by the mutations (Figure 1A) also affect Drp1 helical propagation in solution. In the constant presence of

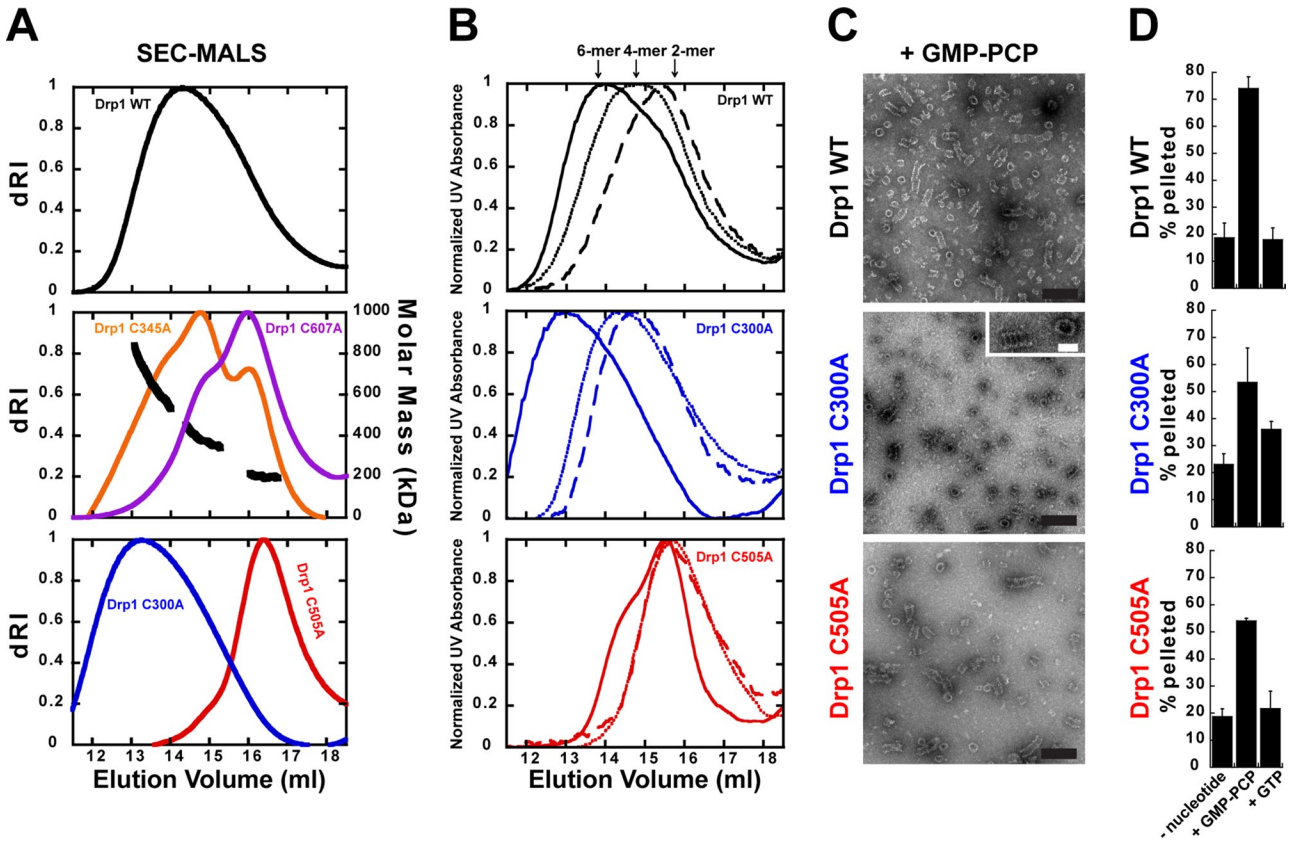


FIGURE 4: Drp1 polymerization equilibria and mutants. (A) SEC-MALS analyses of Drp1 WT and mutants. Middle, determined molar mass profiles (black dots) for discernible peak regions of the broad Drp1 elution profile. Differential refractive indices (dRI) are normalized and plotted against elution volume (ml). (B) SEC elution profile shifts for Drp1 WT and mutants as a function of loaded protein concentration. Solid, dotted, and dashed line profiles represent loaded protein concentrations of 10, 5, and 2.5 μM, respectively. Normalized ultraviolet light absorbance measured at 280 nm is plotted against elution volume (ml). Arrows point to corresponding peak positions for Drp1 dimers, tetramers, and hexamers. (C) EM images of Drp1 WT and mutant helical polymers formed in the presence of GMP-PCP in solution. Scale bar, 200 nm. Middle, inset, magnified image of a Drp1 C300A helical polymer. Scale bar (white), 50 nm. (D) Percentage Drp1 sedimented by high-speed centrifugation in the absence or presence of GMP-PCP or GTP for WT and mutants. Averages ± SD for $n \geq 3$.

GTP, however, the two mutants behaved very differently. Drp1 C505A, similar to WT, did not propagate into sedimentable higher-order polymers, consistent with the role of GTP hydrolysis in limiting Drp1 self-assembly (Figure 4D, bottom). Drp1 C300A, on the other hand, retained a significant fraction of sedimentable higher-order polymers, which appeared resistant to disassembly by GTP hydrolysis (Figure 4D, middle). Consistent with this observation, Drp1 C300A exhibited a significantly higher basal GTPase activity than both Drp1 C505A and WT (Supplemental Figure S5). From these data, we conclude that mutations C300A and C505A, under physiological conditions in solution, differentially alter Drp1 polymerization equilibria by shifting them in opposite directions to supra-oligomers and dimers, respectively.

### Dimers potentiate Drp1-mediated membrane remodeling both in vitro and in vivo

Our current impressions of how Drp1 functions in mitochondrial division stem largely from parallels drawn to dynamin in endocytic vesicle scission (Bui and Shaw, 2013). For instance, Drp1 multimerization in solution (tetramerization or higher), by analogy with dynamin (Ramachandran *et al.*, 2007), is believed to be essential for the nucleation of its higher-order self-assembly on membranes (Chang *et al.*, 2010).

In a marked departure from dynamin, we found that dimeric Drp1 C505A bound CL-containing liposomes equally well as Drp1 C300A and Drp1 WT (Figure 5A). Because the conventional centrifugation assay cannot reliably distinguish between solution-suspended oligomers of Drp1 and its membrane-bound polymers, we developed a Förster resonance energy transfer (FRET)–based approach to assay directly for Drp1–membrane association. To this end, we used the lone B-insert tryptophan (Trp) residue, W552, as a FRET energy "donor" for "acceptor" 1,2-dioleoyl-*sn*-glycero-3-phosphoethanolamine-*N*-(5-dimethylamino-1-naphthalenesulfonyl) (Dansyl-PE) lipid molecules distributed randomly across the CL-containing membrane surface. Identical increases in Dansyl emission intensity upon Trp excitation for all three species revealed comparable membrane association (Figure 5A, left), a property also reflected in spin-sedimentation profiles (Figure 5A, right).

Remarkably, however, Drp1 C505A was significantly more active in tubulating CL-containing membranes than both Drp1 C300A and Drp1 WT (Figure 5B). Consistent with this observation, the assembly-stimulated GTP hydrolysis rate of Drp1 C505A was also

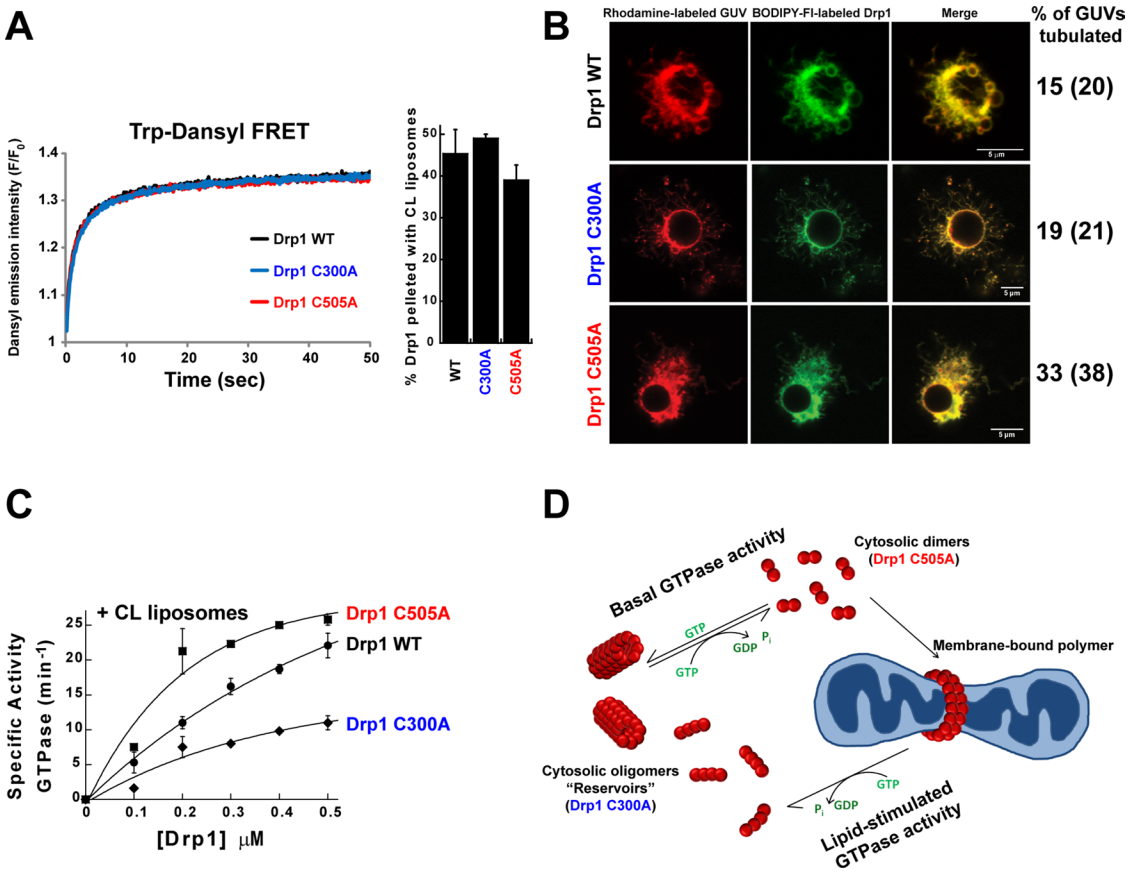


FIGURE 5: Drp1 dimers potentiate membrane remodeling. (A) Left, FRET-sensitized, time-dependent increase in Dansyl emission intensity upon Trp excitation plotted as $F/F_0$, where $F_0$ is the background Dansyl emission intensity before Drp1 addition, and $F$ is Dansyl emission intensity at time $t$ after Drp1 addition. Representative traces. Right, percentage Drp1 sedimented by high-speed centrifugation after incubation with CL-containing liposomes. Averages ± SD for $n \geq 3$. (B) Representative confocal fluorescence images of membrane tubules extracted by BODIPY-Fl–labeled Drp1 and mutants (green) from rhodamine–labeled PC/CL GUVs (red). Scale bar, 5 μm. The relative efficiency of GUV tubulation is quantified and indicated as percentage GUVs tubulated. More than 25 GUVs were scored for each Drp1 species from three independent experiments. Numbers in parentheses represent those from PC/PE/CL GUVs. (C) Specific activity of Drp1 and mutants on CL-containing liposomes (150 μM total lipid) as a function of protein concentration. Averages ± SD for $n \geq 3$. (D) Model for Drp1 polymerization equilibria and morphology. Drp1 C505A exists predominantly as "dimers" in the cytosol, whereas Drp1 C300A is stabilized as "supra-oligomers."

significantly greater than that of Drp1 WT when assayed at low limiting protein concentrations (Figure 5C). Lipid stimulation of Drp1 C300A, on the other hand, was dramatically impaired (Figure 5C). Thus the extents of Drp1-mediated membrane remodeling and lipid-dependent GTPase stimulation appeared anticorrelated to Drp1 oligomerization propensity in solution. In other words, the larger the Drp1 oligomer in solution, the lower was its potential to constitute remodeling-competent higher-order polymers on membranes.

From these data, we conclude that Drp1 exists in dynamic equilibrium between two morphologically distinct oligomeric states, one in solution and the other on the membrane, which equilibrate via a dimeric assembly intermediate (Figure 5D). Drp1 C505A, stabilized as minimal dimers in solution, can thus readily reorganize on the membrane to form the distinct membrane-associated polymers required for membrane remodeling. By contrast, in both Drp1 WT and C300A, this reorganization presumably entails, first, disassembly of the preexisting solution oligomers into dimers and, further, subsequent reassembly of the dimers into membrane-associated polymers to engage in membrane remodeling.

If the foregoing model for Drp1 function holds true, Drp1 C505A should be considerably more active than Drp1 C300A in supporting mitochondrial division, when each is expressed to a comparable level in Drp1-knockout (KO) cells. Indeed, dimeric Drp1 C505A was significantly more effective than supra-oligomeric Drp1 C300A in rescuing the mitochondrial fission defect (Figure 6 and Supplemental Figure S6). Oligomerization morphology and equilibria thus modulate Drp1 function in mitochondrial membrane remodeling both in vitro and in vivo.

## DISCUSSION

The data presented here significantly advance our understanding of Drp1's mechanism in mitochondrial division and, of importance, reconcile some disparate findings that have been in the field since its inception. Early studies on purified yeast Dnm1p indicated that the minimal subunit of Dnm1p under physiological conditions is a dimer (Ingerman *et al.*, 2005; Bhar *et al.*, 2006). By contrast, mammalian Drp1 was shown to be a tetramer (Yoon *et al.*, 2001; Bossy *et al.*, 2010). This difference in oligomeric state was attributed to the variable requirements for OMM adaptor proteins that exist between the

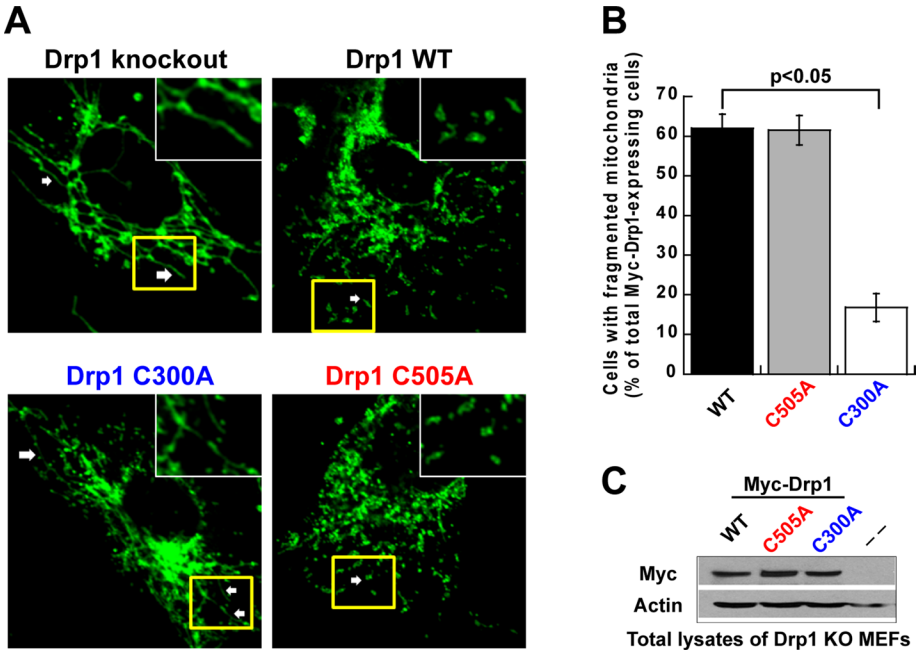


FIGURE 6: Drp1 dimers rescue mitochondrial fission. (A) Confocal fluorescence imaging of mitochondrial morphology in Drp1 KO MEFs expressing either Myc-tagged Drp1 WT or mutants. Block arrows point to either fused or fragmented mitochondria. Inset (white box) shows a magnified view of boxed region (yellow) within each representative cell image. (B) Quantification of mitochondrial fission in Drp1 KO MEFs expressing either Myc-tagged Drp1 WT or mutants. More than 100 Myc-positive cells from three independent experiments were scored for each sample. Data are represented as mean ± SEM. (C) Representative Western blot showing expression levels of Myc-tagged Drp1 WT and mutants in transfected Drp1 KO MEFs. Untransfected cell lysate (– –) was used as negative control, with actin serving as loading control for total protein.

two types of organisms (Bhar *et al.*, 2006; Chan, 2012). We show that human Drp1 under physiological conditions exists in dynamic equilibrium between multiple oligomeric states in solution and propagates in quantized dimeric increments. A similarly broad SEC elution profile observed previously for Dnm1p (Ingerman *et al.*, 2005) may indeed reflect similar dynamics. We conclude that Dnm1p and Drp1 are both minimal dimers in solution.

Our data suggest that CL-enriched microdomains constitute lipid targets that specifically recruit Drp1 to the OMM. However, Drp1 is also recruited to peroxisomal membranes, whose CL content in mammalian cells, although considered negligible, is uncertain (Schumann and Subramani, 2008; Schrader *et al.*, 2012). Enriched in the peroxisomes of yeast, CL has not been biochemically detected in the peroxisomes of mammalian cells (Fujiki *et al.*, 1982; Zinser *et al.*, 1991; Leber *et al.*, 1994; Wriessnegger *et al.*, 2007). However, the recent discovery of mitochondria-derived vesicles that deliver selective protein cargo from the OMM to peroxisomes suggests that CL may indeed be cotransported to peroxisomes via these vesicular membrane carriers (Neuspiel *et al.*, 2008; Schumann and Subramani, 2008). In the absence of irrefutable evidence that supports a role for CL in Drp1 peroxisome recruitment, we speculate that PA, a negatively charged lipid enriched in maturated peroxisomes, with biophysical properties similar to CL and also capable of stimulating Drp1 (Supplemental Figure S1A), plays a corresponding role (Athenstaedt and Daum, 1999; Guo *et al.*, 2007; Mileykovskaya and Dowhan, 2009; Mileykovskaya *et al.*, 2009). Containing a significant fraction of membrane cholesterol, peroxisomal membranes may similarly constitute PA-enriched "rafts," which in turn recruit Drp1 (Woudenberg *et al.*, 2010).

If a direct lipid interaction permits Drp1 association with mitochondrial and peroxisomal membranes as suggested, how can we reconcile the essential roles of membrane-anchored Drp1 adaptors Fis1, Mff, and MiD49/51 in Drp1 recruitment in vivo? It is plausible that a "coincidence detection" of both membrane CL and adaptors at mitochondrial division sites may enhance Drp1 binding to the mitochondria in a synergistic manner and at lower CL concentrations generally found at the OMM (McMahon and Gallop, 2005). It is also plausible that adaptors serve a regulatory role in the Drp1 mechanism by functioning across various checkpoints in the Drp1 oligomerization and GTP hydrolysis cycles (Figure 5D), either upstream or downstream of direct Drp1-membrane interactions. Interestingly, Fis1 and Mff localize to both mitochondrial and peroxisomal membranes and may function in a similar capacity at these distinct membrane compartments to recruit and differentially regulate Drp1 (Schrader *et al.*, 2012; Shen *et al.*, 2014). MiD49/51, restricted to the mitochondria, on the other hand, may exhibit functions that are considerably different from those of Mff and Fis1, as suggested by recent studies (Palmer *et al.*, 2011, 2013; Koirala *et al.*, 2013; Loson *et al.*, 2014; Richter *et al.*, 2014). Elucidation of the specific roles of adaptor proteins in the Drp1 mechanism awaits further examination.

Our studies reveal that under physiological conditions, Drp1 constitutes two morphologically distinct helical polymers. One is a tightly constricted polymer ~50 nm in diameter stabilized by GTP binding in solution, and the other is a relaxed polymer ~100–150 nm in diameter that circumscribes constricted mitochondrial membranes. A lack of pronounced membrane constriction in the membrane-bound polymer upon GMP-PCP addition (i.e., from a starting diameter of ~100–150 nm down to ~30–50 nm found for Drp1 helices in solution) indicates that GTP binding has differential effects on Drp1 molecules suspended in solution versus those bound to lipid. The coexistence of these distinct polymeric populations in vitro, however, correlates well with early observations of punctate yet mobile Dnm1p-GFP structures in the yeast cytosol present alongside discrete Dnm1p foci on the mitochondrial surface (Naylor *et al.*, 2006).

With the characterization of two newly identified mutants, Drp1 C300A and Drp1 C505A, that exhibit dramatically altered oligomerization propensities relative to WT, we further demonstrate that solution dimers, and not multimers, potentiate the reorganization and reassembly of Drp1 on mitochondrial membranes for remodeling and fission. Of interest, the respective locations of the two mutations in the Drp1 crystal structure (Figure 1A) correlate well with their differential effects on Drp1 oligomerization. C505 is located at self-assembly interface 3 of the Drp1 "stalk" involved in stabilizing lateral dimer–dimer contacts in the helical polymer (Frohlich *et al.*, 2013). C300, on the other hand, is positioned at a critical flexion point in the G domain–BSE interface that is responsive to nucleotide-dependent conformational changes originating at the opposite G domain dimerization interface (Wenger *et al.*, 2013). Not

surprisingly, mutations C300A and C505A alternately stabilize or destabilize self-assembly in Drp1, respectively.

In contrast to C505A, all other mutations that reportedly stabilize Drp1 as a dimer in solution also significantly impair function. It is important to note that unlike the charge neutral C505A substitution, all such mutations involve either elimination of a critical surface charge (R403A in Drp1) or introduction of a new surface charge (E490R in Drp1, G385D and G436D in Dnm1p; Ingerman *et al.*, 2005; Ford *et al.*, 2011; Frohlich *et al.*, 2013) that disrupts key ionic interactions necessary for higher-order Drp1 self-assembly. Regardless of such differences, the unaffected membrane binding of Drp1 C505A observed in vitro is in general agreement with the uninhibited mitochondrial recruitment of dimeric Dnm1p G385D reported previously (Bhar *et al.*, 2006). These results further establish that multimerization in the cytosol is not essential for, and is indeed counterproductive to, Drp1 mitochondrial recruitment.

On the basis of a direct correlation between the differential biochemical/biophysical properties of Drp1 C300A and Drp1 C505A on CL-containing membranes in vitro and their corresponding efficacies in supporting mitochondrial fission in vivo, we propose that CL-enriched "contact sites" constitute specific lipid targets for Drp1 activation, as well as the concerted remodeling of the mitochondrial double membrane. Coincidence detection of OMM adaptor proteins at these "contact sites" may accelerate Drp1 retention and reorganization on the OMM for fission. We speculate that CL-enriched "contact sites" exist spatially overlapped with mitochondrial constriction sites generated by tubular endoplasmic reticulum membrane contact, previously shown to recruit Drp1 (Friedman *et al.*, 2011).

On the basis collectively of the foregoing data, we propose that Drp1 polymers found in the cytosol function primarily as "reservoirs" primed to generate "fission-competent dimers" for mitochondrial recruitment and remodeling. The priming transitions presumably occur either through the action of basal GTP hydrolysis and/or via the effect of Drp1 adaptor proteins localized at the OMM. We further speculate that the various posttranslational modifications of Drp1 (phosphorylation, S-nitrosylation, etc.) that govern function in vivo (Chang and Blackstone, 2010) do so via regulation of Drp1 polymerization dynamics.

## MATERIALS AND METHODS

### Expression, purification, and fluorescent labeling of Drp1

Full-length human Drp1 isoform 3 (699 amino acid residues) subcloned in pRSET C (Life Technologies, Carlsbad, CA) was expressed as an N-terminal polyhistidine-tagged recombinant protein in *Escherichia coli* and purified to apparent homogeneity using a combination of nickel-nitriloacetic acid metal ion affinity and DEAE anion exchange chromatographies as described in detail in the Supplemental Methods. Mutations were introduced by PCR-based QuikChange mutagenesis (Agilent Technologies, Santa Clara, CA) and confirmed by automated DNA sequencing. Protein concentration was determined by absorbance using a molar absorptivity coefficient $\varepsilon_{280}$ of 42,860 $M^{-1}$ $cm^{-1}$ for Drp1.

Drp1 was labeled with a thiol-reactive BODIPY-Fl derivative as previously described for dynamin (Ramachandran *et al.*, 2007). The stoichiometry of labeling, determined using a molar absorptivity coefficient of 76,000 $M^{-1}$ $cm^{-1}$ at 502 nm for BODIPY-Fl, was ~2 mol dye/mol protein. Unlabeled and BODIPY-Fl-labeled Drp1 were aliquoted and stored at –80°C in buffer containing 10% (vol/vol) glycerol.

### Preparation of liposomes and lipid nanotubes

All lipids were purchased from Avanti Polar Lipids (Alabaster, AL). Liposomes composed of 25 mol% bovine heart CL, 35 mol% 1,2-dioleoyl-*sn*-glycero-3-phosphoethanolamine (DOPE; PE), and 40 mol% 1,2-dioleoyl-*sn*-glycero-3-phosphocholine (DOPC; PC) were prepared by extrusion (21 times) through polycarbonate membranes of 400-nm pore diameter according to standard protocols (Avanti Polar Lipids). An equivalent mole fraction of other negatively charged lipids replaced CL for the lipid screen as noted in the Supplemental Methods. In liposomes containing <25 mol% CL, DOPE was maintained at 35 mol%, and DOPC made up the remainder. For Drp1-membrane Trp-Dansyl FRET measurements, 10 mol% of Dansyl-PE replaced an equivalent mole fraction of DOPC. Pure PS liposomes were prepared similarly using 1,2-dioleoyl-*sn*-glycero-3-phospho-L-serine (DOPS; PS).

Lipid nanotubes composed of 25 mol% CL, 35 mol% PE (or PC), and 40 mol% C24:1 β-D-galactosyl ceramide were prepared using a sonication protocol described elsewhere (Leonard *et al.*, 2005).

### GTPase assay

Lipid-stimulated hydrolysis of GTP by full-length Drp1 and mutants (0.5 μM final) preincubated on CL-containing liposomes (150 μM final) for 15 min at room temperature before GTP addition was monitored at 37°C over time using a malachite green–based GTPase assay as described earlier (Leonard *et al.*, 2005). GTP (Sigma-Aldrich, St. Louis, MO) was used at a final concentration of 1 mM. $MgCl_2$ and dithiothreitol (DTT) were present at 2 and 1 mM final, respectively. Basal GTP hydrolysis rates for Drp1 WT and mutants were measured similarly but in the absence of lipid.

### Preparation of GUVs and confocal light microscopy

GUVs were electroformed under physiological salt conditions (20 mM 4-(2-hydroxyethyl)-1-piperazineethanesulfonic acid [HEPES], pH 7.5, 150 mM KCl) using home-built, platinum wire electrode chambers as described elsewhere (Montes *et al.*, 2007). The lipid mixture contained either 25 mol% CL, 35 mol% PE, and ~40 mol% PC (PC/PE/CL) or 25 mol% CL and ~75 mol% PC (PC/CL). Both 0.1 mol% rhodamine-PE and 0.5 mol% biotin-PE replacing equivalent mole fractions of DOPC were included, respectively, for fluorescence imaging and GUV immobilization on streptavidin (Sigma-Aldrich)-coupled, biotin-LC-bovine serum albumin–coated (Thermo Scientific, Rockford, IL) LabTek II chambered coverslides prepared according to published protocols (Yildiz *et al.*, 2003). Still images were captured using a 60× oil-immersion objective mounted on an Olympus FV1000 IX81 confocal microscope (Olympus USA, Melville, NY). For visualization of Drp1-mediated membrane remodeling, unlabeled and BODIPY-Fl–labeled Drp1 were premixed at a molar ratio of 3:2 and diffused into the imaging chamber to achieve a final protein concentration of 0.5 μM. The relative efficiency of membrane tubulation by Drp1 WT and mutants was quantified and represented as percentage GUVs tubulated. More than 25 GUVs were scored for each sample from three independent experiments. All procedures and experiments were conducted at room temperature.

### EM

Drp1 WT and mutants (2 μM final) were incubated with GMP-PCP (1 mM final), CL-containing liposomes (50 μM total lipid), or both, in buffer containing 20 mM HEPES, pH 7.5, 150 mM KCl, 2 mM $MgCl_2$, and 1 mM DTT for 30 min at room temperature before deposition on carbon-coated copper EM grids for 2% uranyl acetate staining. Negative-stain EM images were obtained using a Tecnai Spirit BioTwin transmission electron microscope (FEI, Eindhoven, Netherlands) operated at 100 keV with a LaB6 filament. Images were captured on a Gatan US4000 UHS charge-coupled device

(CCD) camera (4k × 4k) (Gatan, Warrensdale, PA). EM images of Drp1 on pure PS liposomes and CL-containing lipid nanotubes were obtained similarly. GMP-PCP was purchased from Sigma-Aldrich.

### SEC-MALS

Drp1 WT and mutants were fractionated on a Superose 6 10/300 GL SEC column (GE Healthcare, Piscataway, NJ) in buffer containing 20 mM HEPES, pH 7.5, 150 mM KCl, and 1 mM DTT and analyzed in-line using tandem miniDAWN Treos MALS and Optilab rEX differential refractive index detectors (Wyatt Technologies, Santa Barbara, CA). Data analysis was accomplished using the ASTRA 6.1 software package (Wyatt Technologies). Drp1 WT and mutants were each loaded at 10 µM in a total volume of 500 µl for molar mass determinations. Protein concentration was varied as indicated for examining concentration-dependent shifts in elution profile.

Molar mass determination by SEC alone relies on calibration against protein reference standards (typically globular proteins) for size and the relative elution position of the molecule of interest, with inherent assumptions of globular shape for the molecule and inertness to interactions with the sizing matrix (column resin) that may ultimately influence its elution profile. This can often lead to erroneous molar mass determinations, especially for nonglobular (asymmetric, elongated), reversibly oligomerizing protein species such as Drp1 and dynamin. However, in combination with MALS (SEC-MALS), measurements are absolute in which the average molecular mass of each eluted species (defined by peaks) is determined in-line based on a direct relationship between protein concentration (measured by in-line refractive index detection), molar mass (protein stoichiometry), and the intensity of scattered light, without calibration against reference standards or assumptions of molecular shape and size (for detailed explanation of this now widely used technique, see Wen *et al.*, 1996; Andersson *et al.*, 2003; Ye, 2006; De *et al.*, 2010).

### Trp-Dansyl FRET assay for Drp1 membrane binding

Binding of Drp1 WT or mutants to CL-containing liposomes was detected by monitoring FRET between a Trp residue in Drp1 (W552 in the B insert) and Dansyl-PE lipid molecules randomly distributed on the membrane surface using a SX20 stopped flow spectrometer (Applied Photophysics, Leatherhead, United Kingdom). The final concentrations of Drp1 and lipid after mixing were 0.4 and 20 µM respectively. Drp1 Trp was excited at 280 nm, and Dansyl emission intensity was monitored between 460 and 540 nm, using a 500FS40-25 standard bandpass filter (Andover Corporation, Salem, NH). The FRET-dependent increase in Dansyl emission intensity was recorded at 0.1-s time intervals. Experiments were maintained at 25°C using a circulating water bath.

It is important to note that the remaining two Trp residues present in Drp1, W90 in the G domain and W699 as the terminal residue of isoform 3, are positioned too far from the membrane surface to be able to participate in Trp-Dansyl FRET ($R_0 \approx 21$ Å, where $R_0$ is the characteristic distance for a FRET pair at which the efficiency of energy transfer [*E*] is 50%; Gustiananda *et al.*, 2004). Owing to the inverse-sixth-power distance dependence of FRET, *E* rapidly approaches zero as the distance separating the FRET pair increases to $1.5R_0$, or ~32 Å for the Trp-Dansyl pair (Piston and Kremers, 2007).

### Sedimentation assay for Drp1 oligomerization and membrane binding

Drp1 WT and mutants (5 µM protein final) were incubated with or without CL-containing liposomes (500 µM lipid final) in buffer containing 20 mM HEPES, pH 7.5, 150 mM KCl, 2 mM $MgCl_2$, and 1 mM DTT in the absence or presence of nucleotide (1 mM final) for 30 min at room temperature. Supernatant (S) and pellet (P) fractions were obtained by high-speed centrifugation of the samples at 20,800 × *g* in a refrigerated microcentrifuge maintained at 4°C. Densitometry of S and P fractions after SDS–PAGE and Coomassie staining was performed using ImageJ (National Institutes of Health, Bethesda, MD). Drp1 pelleted is presented as percentage of total.

### Cell culture and immunocytochemistry

Drp1-KO mouse embryonic fibroblasts (MEFs; Wakabayashi *et al.*, 2009) were maintained in DMEM supplemented with 10% (vol/vol) heat-inactivated fetal calf serum and 1% (vol/vol) penicillin/streptomycin at 37°C in 5% $CO_2$/95% air. Cells were transfected with 2 µg of plasmid DNA encoding either Myc-tagged Drp1 WT or mutants (pCMV-Myc; Clontech, Mountain View, CA) using *Trans*IT-2020 Transfection Reagent (Mirus Bio, Madison, WI) according to the manufacturer's protocol.

Cells cultured on coverslips were washed with cold phosphate-buffered saline (PBS), fixed in 4% formaldehyde, and permeabilized with 0.1% Triton X-100. After incubation with 2% normal goat serum (to block nonspecific staining), fixed cells were incubated overnight at 4°C with rabbit anti-Tom20 (1:500; Santa Cruz Biotechnology, Santa Cruz, CA) and mouse anti-Myc (1:500; Santa Cruz Biotechnology) primary antibodies. Cells were washed with PBS and incubated with Alexa Fluor 488–conjugated anti-rabbit and Alexa Fluor 568–conjugated anti-mouse secondary antibodies (1:500; Invitrogen, Carlsbad, CA) for 60 min at room temperature. This was followed by incubation with Hoechst dye (1:10,000; Invitrogen) for 10 min. Coverslips were mounted on glass slides and imaged by confocal fluorescence microscopy using an Olympus FV1000 IX81 confocal microscope (Olympus USA).

To quantify mitochondrial fragmentation, cells were immunostained with anti-Tom20 and anti-Myc antibodies as described. Mitochondrial morphology was then examined in >100 Myc-positive cells for each sample from three independent experiments. The percentage of Myc-Drp1–expressing cells displaying fragmented, punctiform mitochondria, as exemplified by Myc-Drp1 WT–expressing cells in Figure 6A, relative to the total number of Myc-expressing cells was quantified.

### Western blotting

Drp1 KO MEFs were transfected with the indicated plasmids as described. Total protein was harvested 24 h after transfection, and protein concentration was determined by Bradford assay. From each sample 30 µg of total protein was resuspended in Laemmli buffer, resolved by SDS–PAGE, and transferred onto nitrocellulose membranes. Membranes were probed with anti-Myc and anti-actin (Sigma-Aldrich) antibodies (1:1000 dilution for both) followed by visualization using enhanced chemiluminescence.

## ACKNOWLEDGMENTS

This research was supported by American Heart Association Grants 13BGIA14810010 to R.R., 12SDG9130039 to J.A.M., and 12BGIA8800014 to X.Q. and National Institutes of Health R01 Grant GM089853 to H.S.

## REFERENCES

Andersson M, Wittgren B, Wahlund KG (2003). Accuracy in multiangle light scattering measurements for molar mass and radius estimations. Model calculations and experiments. Anal Chem 75, 4279–4291.

Ardail D, Privat JP, Egret-Charlier M, Levrat C, Lerme F, Louisot P (1990). Mitochondrial contact sites. Lipid composition and dynamics. J Biol Chem 265, 18797–18802.

Athenstaedt K, Daum G (1999). Phosphatidic acid, a key intermediate in lipid metabolism. Eur J Biochem 266, 1–16.
Bhar D, Karren MA, Babst M, Shaw JM (2006). Dimeric Dnm1-G385D interacts with Mdv1 on mitochondria and can be stimulated to assemble into fission complexes containing Mdv1 and Fis1. J Biol Chem 281, 17312–17320.
Bossy B, Petrilli A, Klinglmayr E, Chen J, Lutz-Meindl U, Knott AB, Masliah E, Schwarzenbacher R, Bossy-Wetzel E (2010). S-Nitrosylation of DRP1 does not affect enzymatic activity and is not specific to Alzheimer's disease. J Alzheimers Dis 20 (Suppl 2), S513–S526.
Bui HT, Shaw JM (2013). Dynamin assembly strategies and adaptor proteins in mitochondrial fission. Curr Biol 23, R891–R899.
Chan DC (2012). Fusion and fission: interlinked processes critical for mitochondrial health. Annu Rev Genet 46, 265–287.
Chang CR, Blackstone C (2010). Dynamic regulation of mitochondrial fission through modification of the dynamin-related protein Drp1. Ann NY Acad Sci 1201, 34–39.
Chang CR, Manlandro CM, Arnoult D, Stadler J, Posey AE, Hill RB, Blackstone C (2010). A lethal de novo mutation in the middle domain of the dynamin-related GTPase Drp1 impairs higher order assembly and mitochondrial division. J Biol Chem 285, 32494–32503.
Cho DH, Nakamura T, Fang J, Cieplak P, Godzik A, Gu Z, Lipton SA (2009). S-nitrosylation of Drp1 mediates beta-amyloid-related mitochondrial fission and neuronal injury. Science 324, 102–105.
De N, Navarro MV, Wang Q, Krasteva PV, Sondermann H (2010). Biophysical assays for protein interactions in the Wsp sensory system and biofilm formation. Methods Enzymol 471, 161–184.
Elgass K, Pakay J, Ryan MT, Palmer CS (2013). Recent advances into the understanding of mitochondrial fission. Biochim Biophys Acta 1833, 150–161.
Ford MG, Jenni S, Nunnari J (2011). The crystal structure of dynamin. Nature 477, 561–566.
Friedman JR, Lackner LL, West M, DiBenedetto JR, Nunnari J, Voeltz GK (2011). ER tubules mark sites of mitochondrial division. Science 334, 358–362.
Friedman JR, Nunnari J (2014). Mitochondrial form and function. Nature 505, 335–343.
Frohlich C, Grabiger S, Schwefel D, Faelber K, Rosenbaum E, Mears J, Rocks O, Daumke O (2013). Structural insights into oligomerization and mitochondrial remodelling of dynamin 1-like protein. EMBO J 32, 1280–1292.
Fujiki Y, Fowler S, Shio H, Hubbard AL, Lazarow PB (1982). Polypeptide and phospholipid composition of the membrane of rat liver peroxisomes: comparison with endoplasmic reticulum and mitochondrial membranes. J Cell Biol 93, 103–110.
Fuller N, Benatti CR, Rand RP (2003). Curvature and bending constants for phosphatidylserine-containing membranes. Biophys J 85, 1667–1674.
Guo T *et al*. (2007). A signal from inside the peroxisome initiates its division by promoting the remodeling of the peroxisomal membrane. J Cell Biol 177, 289–303.
Gustiananda M, Liggins JR, Cummins PL, Gready JE (2004). Conformation of prion protein repeat peptides probed by FRET measurements and molecular dynamics simulations. Biophys J 86, 2467–2483.
Hauser H, Phillips MC (1973). Structures of aqueous dispersions of phosphatidylserine. J Biol Chem 248, 8585–8591.
Hoppins S, Nunnari J (2012). Cell biology. Mitochondrial dynamics and apoptosis—the ER connection. Science 337, 1052–1054.
Horvath SE, Daum G (2013). Lipids of mitochondria. Prog Lipid Res 52, 590–614.
Ingerman E, Perkins EM, Marino M, Mears JA, McCaffery JM, Hinshaw JE, Nunnari J (2005). Dnm1 forms spirals that are structurally tailored to fit mitochondria. J Cell Biol 170, 1021–1027.
Itoh K, Nakamura K, Iijima M, Sesaki H (2013). Mitochondrial dynamics in neurodegeneration. Trends Cell Biol 23, 64–71.
Kagan VE *et al*. (2005). Cytochrome c acts as a cardiolipin oxygenase required for release of proapoptotic factors. Nat Chem Biol 1, 223–232.
Koirala S, Guo Q, Kalia R, Bui HT, Eckert DM, Frost A, Shaw JM (2013). Interchangeable adaptors regulate mitochondrial dynamin assembly for membrane scission. Proc Natl Acad Sci USA 110, E1342–1351.
Korobova F, Ramabhadran V, Higgs HN (2013). An actin-dependent step in mitochondrial fission mediated by the ER-associated formin INF2. Science 339, 464–467.
Lackner LL, Horner JS, Nunnari J (2009). Mechanistic analysis of a dynamin effector. Science 325, 874–877.
Lackner LL, Nunnari JM (2009). The molecular mechanism and cellular functions of mitochondrial division. Biochim Biophys Acta 1792, 1138–1144.
Leber R, Zinser E, Zellnig G, Paltauf F, Daum G (1994). Characterization of lipid particles of the yeast, *Saccharomyces cerevisiae*. Yeast 10, 1421–1428.
Leonard M, Song BD, Ramachandran R, Schmid SL (2005). Robust colorimetric assays for dynamin's basal and stimulated GTPase activities. Methods Enzymol 404, 490–503.
Li H *et al*. (2013). A Bcl-xL-Drp1 complex regulates synaptic vesicle membrane dynamics during endocytosis. Nat Cell Biol 15, 773–785.
Loson OC, Liu R, Rome ME, Meng S, Kaiser JT, Shan SO, Chan DC (2014). The Mitochondrial fission receptor MiD51 requires ADP as a cofactor. Structure 22, 367–377.
Loson OC, Song Z, Chen H, Chan DC (2013). Fis1, Mff, MiD49, and MiD51 mediate Drp1 recruitment in mitochondrial fission. Mol Biol Cell 24, 659–667.
McMahon HT, Gallop JL (2005). Membrane curvature and mechanisms of dynamic cell membrane remodelling. Nature 438, 590–596.
Mears JA, Lackner LL, Fang S, Ingerman E, Nunnari J, Hinshaw JE (2011). Conformational changes in Dnm1 support a contractile mechanism for mitochondrial fission. Nat Struct Mol Biol 18, 20–26.
Mileykovskaya E, Dowhan W (2009). Cardiolipin membrane domains in prokaryotes and eukaryotes. Biochim Biophys Acta 1788, 2084–2091.
Mileykovskaya E, Ryan AC, Mo X, Lin CC, Khalaf KI, Dowhan W, Garrett TA (2009). Phosphatidic acid and N-acylphosphatidylethanolamine form membrane domains in *Escherichia coli* mutant lacking cardiolipin and phosphatidylglycerol. J Biol Chem 284, 2990–3000.
Mishra N, Kar R, Singha PK, Venkatachalam MA, McEwen DG, Saikumar P (2010). Inhibition of mitochondrial division through covalent modification of Drp1 protein by 15 deoxy-Delta(12,14)-prostaglandin J2. Biochem Biophys Res Commun 395, 17–24.
Montes LR, Alonso A, Goni FM, Bagatolli LA (2007). Giant unilamellar vesicles electroformed from native membranes and organic lipid mixtures under physiological conditions. Biophys J 93, 3548–3554.
Montessuit S *et al*. (2010). Membrane remodeling induced by the dynamin-related protein Drp1 stimulates Bax oligomerization. Cell 142, 889–901.
Naylor K, Ingerman E, Okreglak V, Marino M, Hinshaw JE, Nunnari J (2006). Mdv1 interacts with assembled dnm1 to promote mitochondrial division. J Biol Chem 281, 2177–2183.
Neuspiel M, Schauss AC, Braschi E, Zunino R, Rippstein P, Rachubinski RA, Andrade-Navarro MA, McBride HM (2008). Cargo-selected transport from the mitochondria to peroxisomes is mediated by vesicular carriers. Curr Biol 18, 102–108.
Okamoto K, Shaw JM (2005). Mitochondrial morphology and dynamics in yeast and multicellular eukaryotes. Annu Rev Genet 39, 503–536.
Ong SB, Hausenloy DJ (2010). Mitochondrial morphology and cardiovascular disease. Cardiovasc Res 88, 16–29.
Palmer CS, Elgass KD, Parton RG, Osellame LD, Stojanovski D, Ryan MT (2013). Adaptor proteins MiD49 and MiD51 can act independently of Mff and Fis1 in Drp1 recruitment and are specific for mitochondrial fission. J Biol Chem 288, 27584–27593.
Palmer CS, Osellame LD, Laine D, Koutsopoulos OS, Frazier AE, Ryan MT (2011). MiD49 and MiD51, new components of the mitochondrial fission machinery. EMBO Rep 12, 565–573.
Piston DW, Kremers GJ (2007). Fluorescent protein FRET: the good, the bad and the ugly. Trends Biochem Sci 32, 407–414.
Ramachandran R, Surka M, Chappie JS, Fowler DM, Foss TR, Song BD, Schmid SL (2007). The dynamin middle domain is critical for tetramerization and higher-order self-assembly. EMBO J 26, 559–566.
Richter V, Palmer CS, Osellame LD, Singh AP, Elgass K, Stroud DA, Sesaki H, Kvansakul M, Ryan MT (2014). Structural and functional analysis of MiD51, a dynamin receptor required for mitochondrial fission. J Cell Biol 204, 477–486.
Schlattner U, Tokarska-Schlattner M, Rousseau D, Boissan M, Mannella C, Epand R, Lacombe ML (2014). Mitochondrial cardiolipin/phospholipid trafficking: the role of membrane contact site complexes and lipid transfer proteins. Chem Phys Lipids 179, 32–41.
Schrader M, Bonekamp NA, Islinger M (2012). Fission and proliferation of peroxisomes. Biochim Biophys Acta 1822, 1343–1357.
Schumann U, Subramani S (2008). Special delivery from mitochondria to peroxisomes. Trends Cell Biol 18, 253–256.
Shen Q, Yamano K, Head BP, Kawajiri S, Cheung JT, Wang C, Cho JH, Hattori N, Youle RJ, van der Bliek AM (2014). Mutations in Fis1 disrupt orderly disposal of defective mitochondria. Mol Biol Cell 25, 145–159.
Sorice M, Manganelli V, Matarrese P, Tinari A, Misasi R, Malorni W, Garofalo T (2009). Cardiolipin-enriched raft-like microdomains are essential activating platforms for apoptotic signals on mitochondria. FEBS Lett 583, 2447–2450.

Strack S, Wilson TJ, Cribbs JT (2013). Cyclin-dependent kinases regulate splice-specific targeting of dynamin-related protein 1 to microtubules. J Cell Biol 201, 1037–1051.
Tatsuta T, Scharwey M, Langer T (2014). Mitochondrial lipid trafficking. Trends Cell Biol 24, 44–52.
van Meer G, Voelker DR, Feigenson GW (2008). Membrane lipids: where they are and how they behave. Nat Rev Mol Cell Biol 9, 112–124.
Wakabayashi J, Zhang Z, Wakabayashi N, Tamura Y, Fukaya M, Kensler TW, Iijima M, Sesaki H (2009). The dynamin-related GTPase Drp1 is required for embryonic and brain development in mice. J Cell Biol 186, 805–816.
Wen J, Arakawa T, Philo JS (1996). Size-exclusion chromatography with on-line light-scattering, absorbance, and refractive index detectors for studying proteins and their interactions. Anal Biochem 240, 155–166.
Wenger J, Klinglmayr E, Frohlich C, Eibl C, Gimeno A, Hessenberger M, Puehringer S, Daumke O, Goettig P (2013). Functional mapping of human dynamin-1-like GTPase domain based on x-ray structure analyses. PLoS One 8, e71835.
Woudenberg J *et al*. (2010). Lipid rafts are essential for peroxisome biogenesis in HepG2 cells. Hepatology 52, 623–633.
Wriessnegger T, Gubitz G, Leitner E, Ingolic E, Cregg J, de la Cruz BJ, Daum G (2007). Lipid composition of peroxisomes from the yeast *Pichia pastoris* grown on different carbon sources. Biochim Biophys Acta 1771, 455–461.
Ye H (2006). Simultaneous determination of protein aggregation, degradation, and absolute molecular weight by size exclusion chromatography-multiangle laser light scattering. Anal Biochem 356, 76–85.
Yildiz A, Forkey JN, McKinney SA, Ha T, Goldman YE, Selvin PR (2003). Myosin V walks hand-over-hand: single fluorophore imaging with 1.5-nm localization. Science 300, 2061–2065.
Yoon Y, Pitts KR, McNiven MA (2001). Mammalian dynamin-like protein DLP1 tubulates membranes. Mol Biol Cell 12, 2894–2905.
Youle RJ, van der Bliek AM (2012). Mitochondrial fission, fusion, and stress. Science 337, 1062–1065.
Zinser E, Sperka-Gottlieb CD, Fasch EV, Kohlwein SD, Paltauf F, Daum G (1991). Phospholipid synthesis and lipid composition of subcellular membranes in the unicellular eukaryote *Saccharomyces cerevisiae*. J Bacteriol 173, 2026–2034.